Biomacromolecules

pubs.acs.org/Biomac

Article

Strategic Insights into Engineering Parameters Affecting Cell Type-Specific Uptake of DNA-Based Nanomaterials

Marianna M. Koga,[†] Alice Comberlato,[†] Hugo J. Rodríguez-Franco, and Maartje M. C. Bastings*

Cite This: *Biomacromolecules* 2022, 23, 2586−2594

Read Online

ACCESS | Metrics & More | Article Recommendations | Supporting Information

ABSTRACT: DNA-based nanomaterials are gaining popularity as uniform and programmable bioengineering tools as a result of recent solutions to their weak stability under biological conditions. The DNA nanotechnology platform uniquely allows decoupling of engineering parameters to comprehensively study the effect of each upon cellular encounter. We here present a systematic analysis of the effect of surface parameters of DNA-based nanoparticles on uptake in three different cell models: tumor cells, macrophages, and dendritic cells. The influence of surface charge, stabilizing coating, fluorophore types, functionalization technique, and particle concentration employed is found to cause significant differences in material uptake among these cell types. We therefore provide new insights into the large variance in cell type-specific uptake, highlighting the necessity of proper engineering and careful assay development when DNA-based materials are used as tools in bioengineering and as future nanotherapeutic agents.

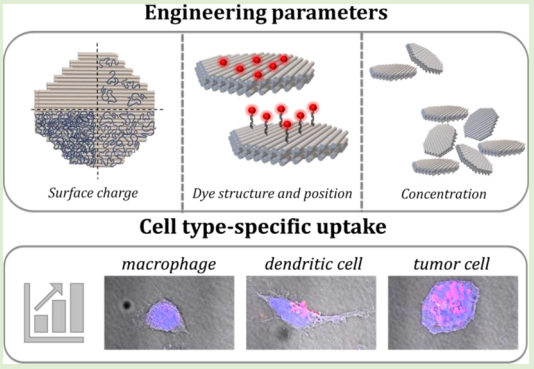

INTRODUCTION

The development of nanoparticles (NPs) as therapeutic drug delivery tools is a prominent field at full speed expansion. DNA-based nanotechnology offers a versatile platform that provides absolute control over the size and shape of the NP, eliminating the size polydispersity issue of traditional polymeric NPs. In particular, in the DNA origami technique, NPs are prepared from a single-stranded scaffold DNA sequence that is folded in a predetermined design by annealing with multiple shorter oligonucleotides (staple strands), exploiting the programmable base-pairing of DNA.[1] Additionally, DNA origami nanostructures are of particular interest now that many stability strategies can be employed, such as coating-based or cross-linking techniques, which protect the NP integrity against low salt strength and nucleases in cell media, and under *in vivo* conditions.[2] Properties such as surface charges can be further manipulated by the type and amount of coating applied. Oligolysine (K10) conjugated with polyethylene glycol (PEG) is one of the most promising off-the-shelf solutions to date: K10-PEG 5 K was shown to effectively stabilize DNA NPs from nuclease degradation *in vitro* and *in vivo*.[3] In addition to that, K10-PEG is a low-cost material that further allows surface charge modulation by altering the ratio of nitrogens (N) in lysines applied to phosphorus (P) in DNA (N:P).

The programmable nature of DNA allows the straightforward incorporation of functional molecules using the classical handle-antihandle (H/AH) approach, where a single-stranded DNA sequence (ssDNA) protruding from the DNA NP hybridizes with its complementary sequence present on the functional molecule to be incorporated or via direct ligation to a ssDNA that makes up the core of the NP.[4] As one of the functionalization possibilities, DNA origami can be designed to work as a structural platform to deliver drugs in a target-specific manner: it offers control over the exact number of molecules of a given substance per carrier, allowing a precise correlation of drug load to treatment efficacy.[5−8] Additionally, by functionalizing NPs with fluorophores, cellular uptake and NP fate can be tracked by multiple techniques such as flow cytometry and microscopy analysis.

The interaction between materials and cells is known for its complexity, as each cell type shows a particular subset of surface receptors and uptake pathways.[9] While *in vitro* particle uptake and delivery of cargo studies are often focused on one single target cell type, for therapeutic translation, the same particles face a diverse population of cells. One current example is drug-delivery studies targeting tumor cells *in vivo*. Besides the malignant cells, the tumor microenvironment also contains immune cells, such as dendritic cells (DCs) and macrophages, which are professional phagocytes that provide rapid clearance of particles in general and can play a decisive role in the tumor microenvironment.[10] Therefore, their

Received: March 4, 2022
Revised: May 20, 2022
Published: May 31, 2022

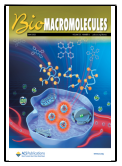

presence in the delivery site of a drug carried by an NP may represent a threat to the success of the treatment by limiting the availability of the compound to the target cells. In addition to that, macrophage activation upon NP uptake may lead to function and phenotypic modifications such as surface receptor expression, which may also alter their uptake patterns and inflammatory responses.[10,11] As for DCs, they are professional antigen-presenting cells that can trigger immunity or immune tolerance based on the conditions they are submitted to during the sampling of the environment.[12] Thus, the consequent type of immune response developed toward the tumor greatly depends on the conditions created by the innate immune cells present in the microenvironment.

DNA-based NPs show great promise as future tools in nanomedicine because of their inherent uniformity and biocompatibility. Their shape and size were found to play a critical role in the efficiency of cellular uptake among different cell types (DCs and endothelial and epithelial cells)[13] and tumor cell models,[14] but no insights into the role of surface parameters have been obtained so far.

Taking advantage of the DNA origami platform, we designed uniform nanostructures with a preferential uptake geometry to explore in more detail the effect of charge, ligand functionalization strategy, and chemical identity on NP cellular internalization. To explore the influence of these critical parameters on the interaction between DNA-based nanomaterials and different cell types, we chose three representative cell models: one of the murine macrophages (RAW 264.7 cells), one of the murine DCs (MutuDC1), and one of the human cancer cells (HeLa). Our results show that not only surface charge matters, but also the fluorophore position and its chemical structure play a major role in the NP uptake in a cell-dependent manner. Moreover, our findings highlight critical steps to avoid false-positive and false-negative data, providing important insights into the influence of design parameters for the future of DNA-based therapeutics.

EXPERIMENTAL SECTION

Removal of LPS from Scaffold p7560. Endotoxin contaminants in the scaffold p7560 solution (Tilibit) were removed with Triton X-114 (Sigma-Aldrich) following a protocol previously described.[15] Briefly, the surfactant Triton X-114 was added at a final concentration of 2% v/v on the purchased scaffold stock, and the solution was gently mixed by inversion at 4 °C for 30 min (step to solubilize endotoxin), subsequently mixed at 37 °C for 5 min at 450 rpm (to induce phase separation), and centrifuged at 37 °C for 30 min at 15,000 rpm. The aqueous fraction on top containing the purified scaffold was transferred to a new tube, and the procedure was repeated four times. The endotoxin amount was measured on the purified scaffold stock using the ToxinSensor Chromogenic LAL Endotoxin Assay Kit (GenScript) following the manufacturer's protocol, to assess a final endotoxin level lower than 0.5 EU mL^{-1}. The purified scaffold was stored at −20 °C.

DNA Origami Self-Assembly. DNA oligonucleotides were purchased from Integrated DNA Technologies (IDT). The DNA origami disk structure was designed with the software cadnano, and self-assembly was performed mixing 10 nM of LPS purified scaffold p7560 (Table S1), 100 nM of core folding staples (Table S2), and 100 nM of variable extra folding staples (see Table S3 for I, Table S4 for H/AH, and Table S5 for H/AH-I for staple sequences corresponding to each structure type) in 1X disk folding buffer (FoB: 5 mM Tris, 1 mM EDTA, 5 mM NaCl, 20 mM $MgCl_2$, pH 8.0), in a total volume of 50 μL. Stock salt solutions for the folding buffer were purchased from Thermo Fisher. The reaction mix was subjected to a thermal annealing ramp using a thermocycler (Biometra Analytik Jena): the mix first incubated at 80 °C for 5 min was followed by a temperature gradient cooling down from 60 to 20 °C in steps of −1 °C per hour and finally stored at 20 °C.

Analytical Agarose Gel Electrophoresis (AGE). The quality of the folding was assessed by AGE; 10 μL of origami solution were mixed with 2 μL of 6X loading dye (Thermo Fisher) and subsequently subjected to AGE (2% agarose, 1X TBE, 15 mM $MgCl_2$, 1X SybrSafe) at 70 V for 90 min in an ice-water bath. Ladder 1kB (N3232L) was purchased from Biolabs. The gels were imaged using a BioRad ChemiDoc MP.

DNA Origami Disk Purification. The DNA origami structures were purified from the excess of staples by PEG precipitation, as previously reported.[16] Briefly, the annealing solutions with folded DNA origami were pooled and mixed in ratio v/v 1:1 with PEG precipitation buffer 2X containing 15% PEG 8000 (VWR), 0.5 M NaCl in 1X disk folding buffer, incubated at room temperature for 30 min, and centrifuged at 16,000 rcf for 40 min at 20 °C. The supernatant containing the extra staples was removed, 1X disk folding buffer was added to the pellet, and the solution was incubated at room temperature overnight. The purification quality was assessed by AGE, and the stock concentration was measured by absorbance at 260 nm using a microvolume spectrophotometer (Quawell Q9000). Purified structures were stored at 4 °C.

Disk Handle Functionalization with Antihandle Dyes. Cy5- or AF647 antihandle DNA sequences (IDT) (Table S6) were annealed on the complementary handles on the disk by adding 3X excess of the dye-functionalized DNA sequence on a PEG-purified H/AH disk stock and incubating the solution at 30 °C for 1 h. Successively, PEG precipitation was repeated to remove the excess of dye-functionalized antihandles. The quality of folding and purification was checked using AGE, and the concentration was measured using a microvolume spectrophotometer (Quawell Q9000).

Coating with K10-PEG. For the coating of the DNA origami, purified origami stock solutions were mixed with a solution of K10-PEG 1 K or 5 K (Alamanda Polymers) of equal volume in 1X folding buffer to obtain a final ratio of nitrogens in lysines of the coating vs phosphates of DNA (N:P ratio) of 0.5:1, 1:1, or 2:1, as previously described,[3] and incubated at room temperature for 30 min. Analytical AGE was performed to assess the coating formation.

Negative-Stain Transmission Electron Microscopy (TEM) Analysis. Eight microliters of DNA origami solution (2 nM of bare or coated DNA origami at different N:P ratios, diluted 1:1 v/v in cell medium) were pipetted onto a CF400-Cu grid (Electron Microscopy Sciences). Before depositing the samples, the grids were subjected to a glow discharge treatment (30 s, 3×10^{-3} A). After 90 s of incubation, the sample was blotted from the grids with filter paper, and then 4 μL of 2% uranyl acetate solution (in H_2O, w/v) were added. Excess solution was immediately removed with filter paper, and the grids were subsequently left to air dry. Imaging was conducted using a Talos L120C TEM operated at 80×10^3 V.

Stability Assay. To assess the stability of the DNA origami in cell medium supplemented with FBS (Figure S1), bare and coated disks were incubated in cell medium with 10% FBS (PAN-Biotech) at 37 °C for 2 h in a total volume of 10 μL. The incubation was stopped through deactivating the FBS nucleases by adding β-mercaptoethanol (1.2 μL, Thermo Fisher) and EGTA (75 mM, 0.8 μL, Thermo Fisher) and incubating at 37 °C for 30 min (final concentration 5 mM EGTA and 10% β-mercaptoethanol). To verify the integrity of the DNA origami disk, the coating was removed to allow the sample to run on AGE: 1 μL of chondroitin sulfate (0.5 M, Carl Roth) was added, and the concentration of $MgCl_2$ was adjusted to restore a concentration of 20 mM. The samples were incubated at 37 °C for 1 h to remove the coating and successively loaded on agarose gel (2% agarose, 1X TBE, 15 mM $MgCl_2$, 1X SybrSafe, run at 70 V for 90 min in an ice-water bath).

Cell Culture. RAW 264.7 and HeLa cells were obtained from the European Collection of Authenticated Cell Cultures (ECACC). The MutuDC1 cell line[17] was kindly provided by Prof. Hans Acha-Orbea, University of Lausanne, Switzerland. The RAW 264.7 and HeLa cell lines were cultured in Dulbecco's modified Eagle's medium high

https://doi.org/10.1021/acs.biomac.2c00282
Biomacromolecules 2022, 23, 2586−2594

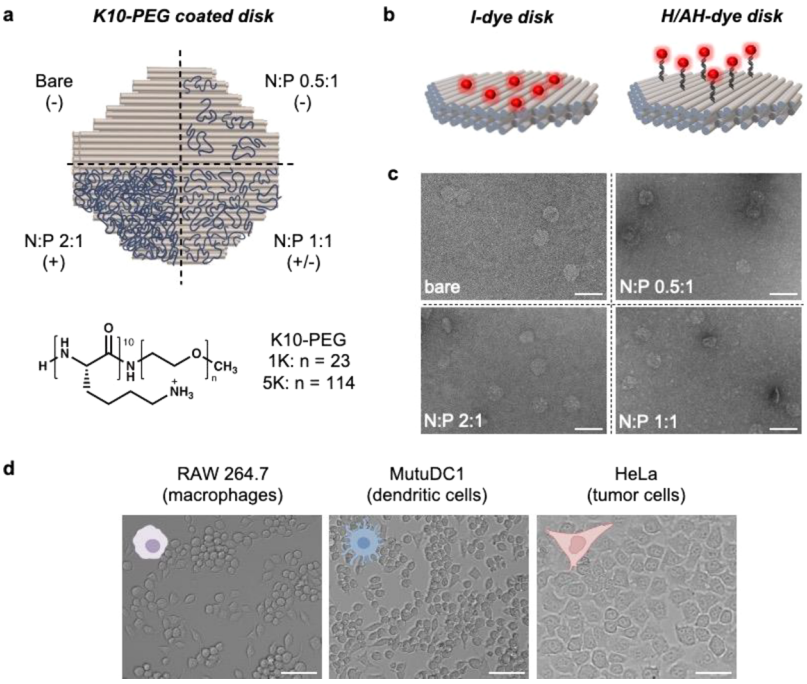

Figure 1. Overview of DNA nanomaterial parameters and cell lines used in this study. (a) Schematic representation of the DNA origami disk NP with different oligolysine-PEG coating N:P ratios (top), where the overall surface charge is indicated between brackets, and the chemical formula of oligolysine-PEG 1 K and 5 K (bottom). (b) Model of the DNA origami disk with integrated-dyes (*I-dye*, left) and handle/antihandle-dye (*H/AH-dye*, bottom) functionalization strategies. (c) TEM images of DNA origami disks with different coating N:P ratios. Scale bars 100 nm. (d) Brightfield microscopy of selected cell lines: RAW 264.7, MutuDC1, and HeLa cell lines. Scale bars 50 μm.

glucose with L-glutamine and sodium pyruvate (Gibco), and the MutuDC1 line was cultured in IMDM-Glutamax (Gibco). Media were supplemented with 10% heat-inactivated fetal bovine serum (FBS Gold, PAN-Biotech) and 100 U mL^{-1} Penicillin−Streptomycin (BioConcept). MutuDC1 medium was additionally supplemented with 10 mM Hepes (Gibco) and 50 μM β-mercaptoethanol (Gibco), as previously described.[18] RAW 264.7 cells were split using the ROTI-Cell PBS/EDTA (Carl Roth), while HeLa and MutuDC1 cells were split using Cell Dissociation Buffer (20 mM HEPES buffer and 5 mM EDTA in PBS, Thermo Fisher) for detaching. All cell lines were kept at maximum 90% confluence and cultured at 37 °C in a humidified 5% CO_2 atmosphere. Cells were analyzed using the microscope Zoe Cell Imager (Biorad), in brightfield mode at 20× magnification.

Uptake Study by Flow Cytometry. Cells were seeded on a 96-well plate (RAW 264.7 and MutuDC1 at 50 × 10^3 cells per well; HeLa at 15 × 10^3 cells per well) and incubated overnight at 37 °C with 5% CO_2 and 95% humidity. For all the assays, the same batch of FBS was used, and cell confluency was confirmed as not higher than 90% before the experiments started. To avoid undesired alteration of NP fluorescence because of environmental conditions, all three cell lines were subjected to the same conditions at the experimental procedure. DNA origami samples were diluted in IMDM-Glutamax supplemented with 10% FBS, at a final concentration of 0.25 nM (if not indicated otherwise) immediately before addition to the cells (50 μL per well) and incubated for 2 h at 37 °C. To remove structures on the cell surface at the end of the incubation, the medium was removed and 50 μL of DNase I (Sigma-Aldrich) diluted in cell medium was added (at a final concentration of 70 U mL^{-1}, as previously reported to degrade also coated disks)[3] and cells were incubated at 37 °C for 1 h. Subsequently, the medium was removed, cells were detached as above mentioned, resuspended in Flow Cytometry Staining (FACS) Buffer (R&D), and transferred to V-bottom plates. Cells were then centrifuged at 500 × *g* for 3 min and washed with cold PBS (Thermo Fisher) followed by Live/Dead Fixable Blue Dead Cell staining (Thermo Fisher) according to the manufacturer's protocol. After washing with FACS Buffer, cells were fixed with 4% paraformaldehyde in PBS (Alfa Aesar) and stored at 4 °C. Cells were analyzed in a LSRII SORP flow cytometer (BD), and data processing was performed using FACS Diva (BD) and FlowJo (Tree Star).

Uptake Study by a Confocal Microscope. Cells were seeded on ibidi 12-well chamber slides (RAW 264.7 and MutuDC1 at 20 × 10^3 cells per well and HeLa at 7.5 × 10^3 cells per well) and incubated overnight in the incubator at 37 °C with 5% CO_2. DNA origami samples were diluted in complete cell medium at a final concentration of 5 nM immediately before addition to the cells (100 μL per well) and incubated for 2 h at 37 °C. To remove structures on the cell surface at the end of the incubation, the medium was removed, and 100 μL of DNase I solution diluted in cell medium was added (at a final concentration of 70 U mL^{-1}, as previously reported to degrade also coated disks[6]), and cells were incubated at 37 °C for 1 h. For controls, the solution was changed with fresh cell medium. Subsequently, the medium was removed, and cells were washed with PBS and fixed with 4% paraformaldehyde in PBS (75 μL, incubating 20 min at room temperature). After washing again with PBS, in case of intracellular staining, cells were permeabilized incubating with 100 μL of 0.1% Triton X-100 (Thermo Fisher) solution in PBS for 10 min at room temperature. After washing with PBS, 100 μL of blocking buffer (5% BSA in PBS) were added and the slide was incubated for 1 h at room temperature. After removing the blocking solution, the corresponding primary antibody solution was added, and the slide was incubated overnight at 4 °C. For early endosome staining, anti-EEA1 antibody (ab109110, abcam) was diluted 1:750 in 5% BSA in PBS. For late endosome staining, anti-RAB7 antibody (ab126712, abcam) was diluted 1:500 in 5% BSA in PBS. After washing with PBS, the secondary antibody goat antirabbit AF488 (ab150077, abcam) was added diluted 1:1000 in PBS at 100 μL per well and the slide was incubated for 1 h at room temperature. After washing with PBS, cells were stained with DAPI solution (50 μL, 300 nM, Thermo Fisher) for 3 min. After two last washes, all the solution was removed from the slide, slide plastic wells were removed, and the glass was left to air dry at room temperature for 15 min. ProLong Glass Antifade Mountant (3 drops, Thermo Fisher) was added on the slide, which was immediately covered with a coverslip and left to air-dry at room temperature for 24 h before analysis.

https://doi.org/10.1021/acs.biomac.2c00282
Biomacromolecules 2022, 23, 2586−2594

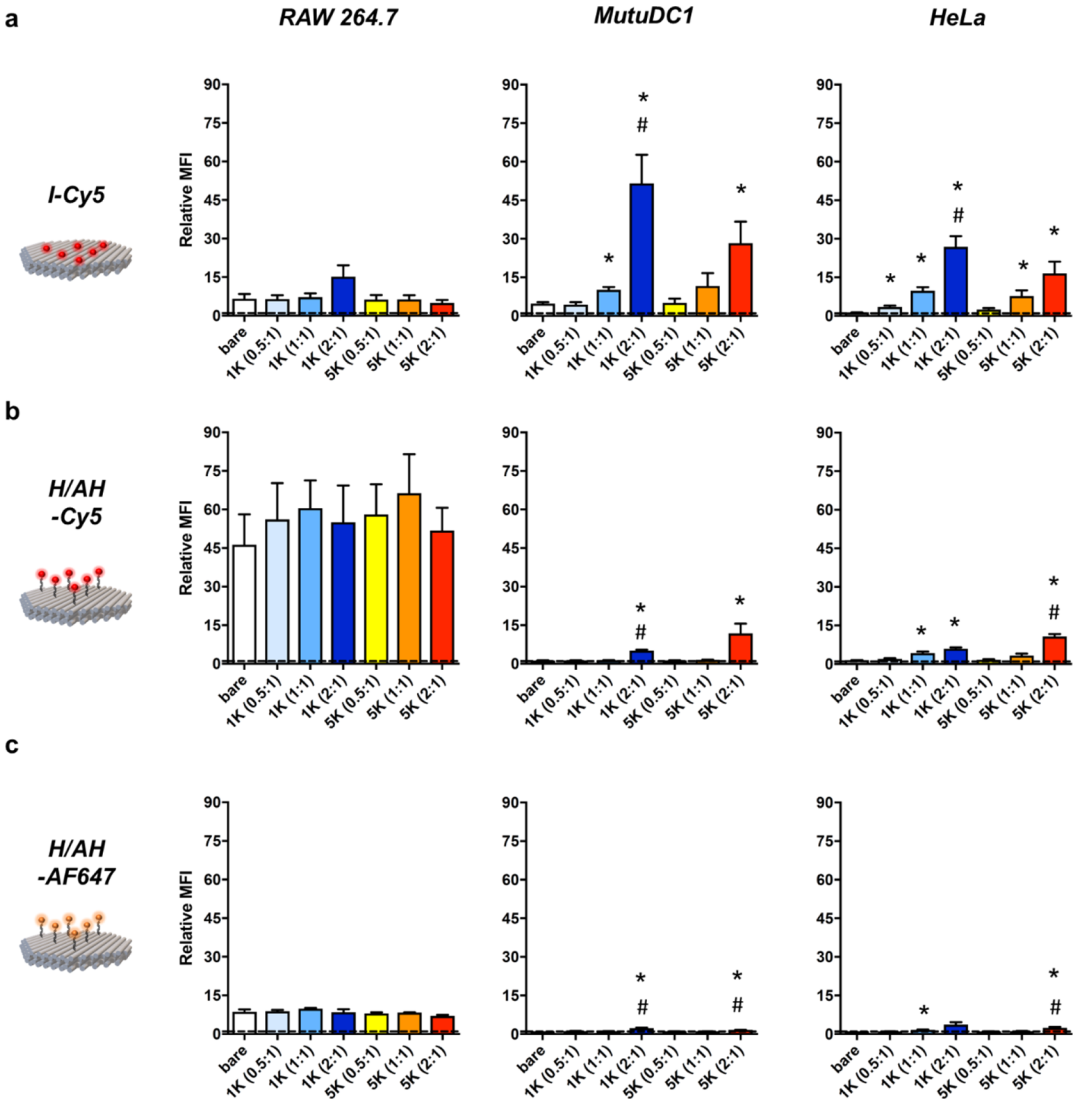

Figure 2. Quantitative analysis of cellular uptake of type (a) I-Cy5, (b) H/AH-Cy5, and (c) H/AH-AF647 disks with K10-PEG 1 K and 5 K at different coating ratios for RAW 264.7, MutuDC1, and HeLa cell lines, assessed by flow cytometry. MFI data are reported compared to the background fluorescence intensity of the corresponding cell line without any treatment as a control (relative MFI). Dashed lines represent the relative MFI of cells incubated with Cy5- or Alexa Fluor 647-functionalized ssDNA under the same conditions. (n = 3). Data are represented as mean +/− SEM values. *P < 0.05 vs bare disk; #P < 0.05 vs PEG-coated neutral disk (1:1), one-way ANOVA.

Samples were imaged using the confocal microscope Zeiss LSM700 Upright with an oil-immersion objective (Zeiss, Plan-apochromat, 63×, NA 1.40, oil). Then, 405, 488, and 639 nm wavelength lasers were used for DAPI, AF488, and Cy5 signals, respectively. BP 445/50, 515−565, and 690/50 filters were applied for DAPI, AF488, and Cy5 emissions, respectively, and imaged with an Axiocam MRm (B/W). Image analysis was performed with the software ImageJ.

Statistical Analysis. Results were presented as mean values ± standard error of the mean (SEM) of at least three independent experiments, with technical triplicates each. Statistical analysis was performed by the one-way analysis of variance (ANOVA) test, followed by Tukey's multiple comparison test, or two-tailed Student's t-test, using GraphPad Prism software (*P < 0.05).

RESULTS AND DISCUSSION

Based on previous insights on how shape and size affect the cellular uptake rate of NPs,[13] we chose a single design of DNA origami structure that could allow rapid uptake: flat solid disks with a diameter of 60 nm.[19] Using DNA nanotechnology, we could exclude variability coming from diverse in-batch NP sizes, which can trigger different uptake pathways among the same samples.[20] The disks were then coated with oligolysine (K10) conjugated to 1 K or 5 K PEG not only to improve biostability[21] but also to additionally modulate surface charge by altering the ratio of positively charged nitrogens (N) in lysines of the coating to negatively charged phosphorus (P) in DNA. As bare DNA origami NPs exhibit a net negative charge, the NP charge can be progressively neutralized by increasing the N:P ratio applied (N:P—0.5:1—negative, 1:1—neutral, or 2:1—positive) (Figure 1a). Importantly, the meshwork provided by the coating does not alter their shape, still allows NP uptake by the cells, and enables DNA handles to be fully accessible.[19]

The DNA origami disks were functionalized with a defined number of dyes, keeping constant ligand pattern positions and changing only the conjugation strategy. To quantify cellular uptake, disks were tagged with six fluorophores in two different conjugation strategies: dyes covalently conjugated to DNA strands used as folding staples of the disks (thus integrated in

https://doi.org/10.1021/acs.biomac.2c00282
Biomacromolecules 2022, 23, 2586−2594

the NP's structure as core modifications, *I-dye* disks), or dyes conjugated to 21 nucleotides antihandle ssDNA strands hybridized by complementarity to ssDNA handles protruding from the disk (handle/antihandle modification, *H/AH-dye* disks) (Figure 1b). The structural integrity and uniformity of the DNA origami disks were verified by AGE (Figure S1) and TEM (Figures 1c and S2). Additionally, the coating and the stability of these structures in cell medium supplemented with 10% FBS were verified by AGE to confirm no differences among the different types of disks existing (Figure S1). The NPs were then presented to three different cell models: RAW 264.7 macrophages, MutuDC1 DCs, and HeLa cancer cells, respectively (Figure 1d).

Cells were incubated with NPs (0.25 nM) for 2 h and then treated with DNase I (70 U mL^{-1}) for 1 h to degrade NPs that could be bound to the cell membrane and not internalized,[13] preventing false-positive uptake results. As an additional control, we used cells incubated with dye-functionalized ssDNA (DNA-dye) to exclude the possibility of NP degradation products to be mistaken as uptake of intact structures.[22] At the equivalent concentration of fluorophores on NPs, the DNA-dye control showed a negligible signal in all cases (Figure 2). Uptake quantification was assessed by flow cytometry, and the uptake threshold was defined relative to the median fluorescence intensity (MFI) of unstimulated cells that were kept in medium only. None of the treatments compromised the cell viability of the three cell lines (Figure S3).

Role of K10-PEG Coating in Cell Type-Dependent NP Uptake. We first compared the general uptake of NPs containing integrated Cy5 fluorophore (I-Cy5 disks) and coated them with K10-PEG 1 K or PEG 5 K providing different surface charges to the NP. We observed that RAW 264.7 cells were less sensitive to variability in charges of the NPs, while MutuDC1 and HeLa cells clearly showed a preference for neutral (N:P − 1:1) and even more for positive surface charge NPs (N:P − 2:1). For HeLa cells, coating the disks with K10-PEG 1 K or PEG 5 K proved fundamental to enable NP uptake. Bare disks are susceptible to degradation due to high concentration of nucleases and low presence of divalent cations in the culture medium;[15] thus a protective coating becomes essential to ensure uptake of DNA NPs when they are exposed to those conditions for longer periods. The fact that uptake of bare disks was not observed by HeLa cells also suggested that those cells performed a slower uptake compared to the other cell types (Figure 2a).

When cells were incubated with disks containing fluorophores conjugated with the handle/antihandle modification (H/AH-Cy5), the disk uptake by RAW 264.7 macrophages was highly increased while the opposite effect was observed for HeLa cells. For MutuDC1, uptake was only observed when H/AH-Cy5 disks were coated with K10-PEG 1 K (2:1) or K10-PEG 5 K (2:1), presenting an overall positive surface charge (Figure 2b). To further explore if the differences observed in the uptake were caused by the presence of protruding DNA sequences on the surface of the NP and not by the H/AH-fluorophore location itself, we designed DNA disks with six integrated dyes plus the same number of nonfunctionalized double-stranded DNA protruding handles from the disks (H/AH-I-Cy5 disks). For all cell lines tested, the disk uptake profile was similar to what was observed when cells were incubated with disks with integrated dyes only, indicating that the dye conjugation strategy is more relevant for NP uptake than handle decoration of the DNA origami (Figure S4). Moreover, this suggested that the observed dramatic change in NP uptake by the RAW 246.7 cells was due to the fluorophore itself, as we explored next.

Role of Dye in Cell Type-Dependent NP Uptake. To test if the uptake of H/AH-Cy5 disks by the RAW 264.7 cells had been facilitated by the increased accessibility of Cy5-conjugated DNA strands protruding from the disks, the cells were preincubated with an excess of free DNA-Cy5 strands to potentially saturate all the membrane receptors involved in their internalization. Although it has been shown that DNA NP uptake occurs by a combination of different endocytic pathways,[23−26] more and more evidence points out to the involvement of scavenger receptors in the uptake of DNA-coated NPs.[14,27] While most of those receptors have been traditionally accounted for the recognition of *self* and *nonself* molecules thus promoting the clearance of dead cells and microbes by macrophages,[28] little is known about their capacity of binding to artificial structures such as DNA NPs. Our results indicated that the preincubation with free DNA-Cy5 strands did not increase the cells' MFI or influence the disk uptake (Figure S5). This, however, did not exclude the possibility of extracellular receptors to be involved in the uptake. As the shape and size play a critical role in the uptake mechanisms employed by the cells, the free dyes probably triggered different uptake pathways than the disks.[29] On the other hand, the data suggested that other features such as the fluorophore's physical and chemical properties in the disks could be involved.

To further explore these factors, we tested the same H/AH functionalization strategy with Alexa Fluor 647 (AF647), showing similar spectral characteristics. In contrast to Cy5, AF647 is negatively charged, and our results showed that uptake of H/AH-AF647 disks by MutuDC1 and HeLa cells was lower compared to H/AH-Cy5 disks, even when the coating ratio was 2:1 (N:P). With respect to the RAW 264.7, we observed that the uptake of H/AH-AF647 was still higher compared to the other two cell lines and did not differ between coating conditions. However, the overall uptake level was significantly reduced and matched the level of I-Cy5 disks, suggesting that the chemical structure itself influences cell surface receptor binding. Indeed, both dyes exhibit a typical cyanine structure with the heterocyclic system, but with an additional long alkyl chain and sulfonyl hydroxide group in AF647 compared to Cy5 (Figure 2c). Taken together, these results suggested a clear preference for the chemical structure of the Cy5 dye and possible implications when it is exposed through handles for the uptake of NPs by RAW 264.7 macrophages. It also implies that when the NPs are designed as drug delivery devices, the chemical structure of the drug may also influence their uptake, which adds another variable to be considered. Nonetheless, further investigation is needed to fully understand the mechanisms behind different DNA NP uptake in each cell type.

Our data emphasize the overall cell-type-dependent aspect of NP uptake. While "fast-eaters" as macrophages and DCs do not directly require material stabilization, fluorophore conjugation design needs to be carefully addressed as the traditional H/AH hybridization strategy combined with the chemical structure of the presented molecule opens an opportunity to discriminate preferential uptake between cell types. Additionally, providing a positively charged structure through coating manipulation can tune the DNA NP surface

https://doi.org/10.1021/acs.biomac.2c00282
Biomacromolecules 2022, 23, 2586−2594

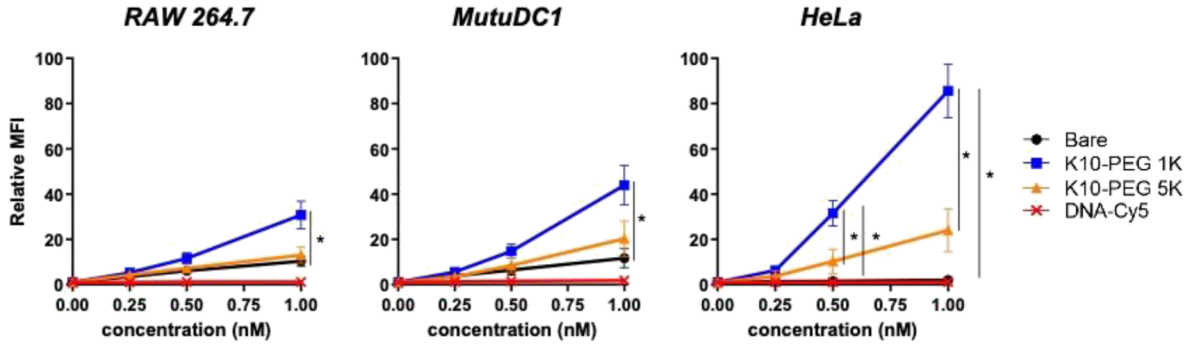

Figure 3. Dose−response curves of cellular uptake of I-Cy5 disks by RAW 264.7, MutuDC1, and HeLa cell lines assessed by flow cytometry. MFI data are reported compared to the background fluorescence intensity of the corresponding cell line without any treatment as a control (relative MFI). (n = 3). Data are represented as mean +/− SEM values. *P < 0.05, one-way ANOVA

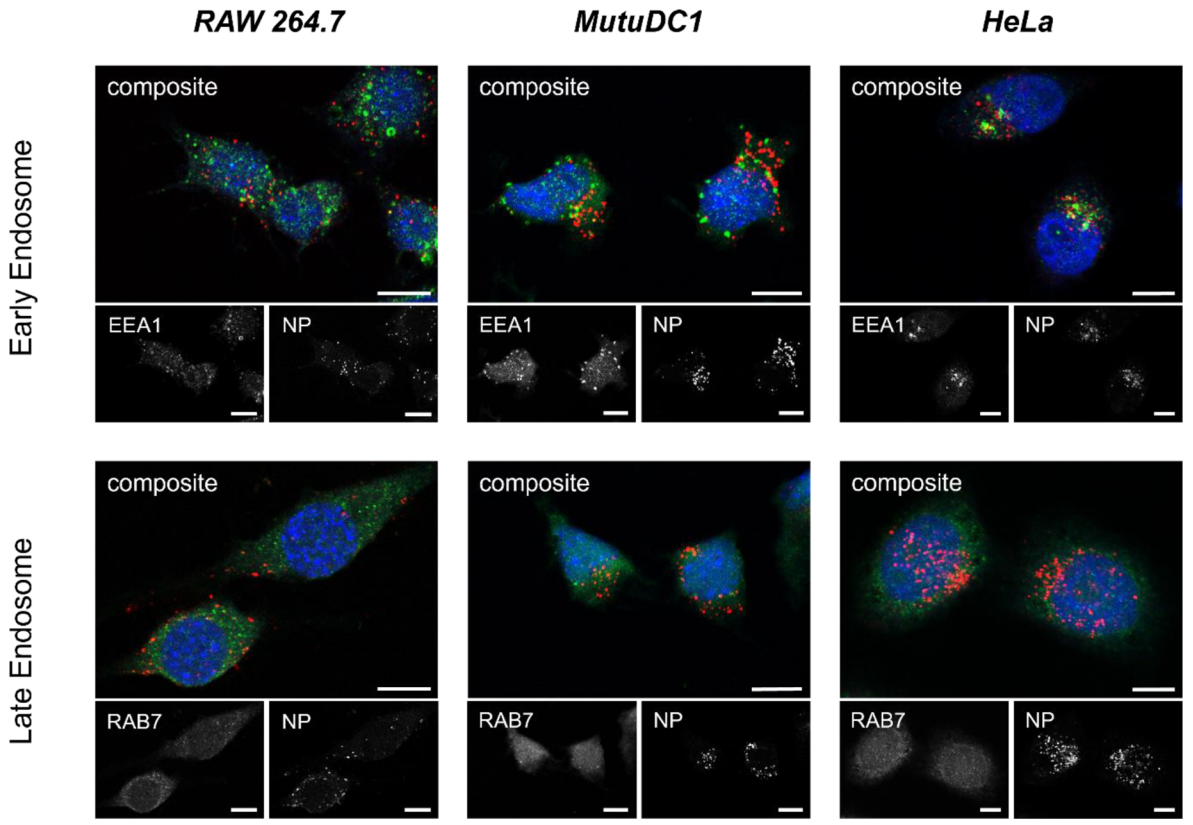

Figure 4. Confocal microscopy analysis of cellular uptake of I-Cy5 disks at 5 nM and coated with K10-PEG 5 K by RAW264.7, MutuDC1, and HeLa cell lines, after DNAse treatment. Confocal microscopy images of single cells overlapped with nuclei in blue (DAPI), early (EEA1) or late endosome (RAB7) in green, and Cy5-labeled disks (NP) in red. Full overview of all the samples is reported in Figures S6−S8. Scale bars 10 μm.

properties, bypassing poor uptake, though at the cost of its selectivity.

Uptake versus Membrane Binding of DNA NPs: A Matter of Concentration. Because neutral I-Cy5 disks coated with K10-PEG 1 K or K10-PEG 5 K (N:P ratio 1:1) exhibited comparable uptake behavior between the three cell lines, we selected these parameters for comparative purposes to next explore the importance of NP concentration for cellular uptake among the different cell lines. Figure 3 shows a clear correlation between NP concentration and uptake of K10-PEG-coated disks. This increased uptake was even more pronounced when NPs were coated with K10-PEG 1 K, particularly for HeLa cells. This observation matches with previous NP studies showing an inverse correlation between the PEG chain length and particle uptake.[30] Higher concentrations of bare disks had little impact on uptake by RAW 264.7 and MutuDC1, whereas uptake of bare disks by HeLa cells was not observed even at a concentration of 1 nM, confirming differential uptake rates by different cell types. These results clearly show the importance of coating the NPs in cases where the target cells perform poor or slow uptake. We confirmed by confocal microscopy that after 2 h of uptake, NP fluorescence colocalized with early and late endosomes in RAW 264.7 and MutuDC1. For HeLa cells, colocalization was more pronounced in the early endosome, confirming a differential kinetic of uptake by these cells (Figures 4 and S6−S8).

Fluorescent dyes resulting from degradation of DNA structures being taken up by cells could be misinterpreted as intact nanostructures, as was previously reported by Lacroix

https://doi.org/10.1021/acs.biomac.2c00282
Biomacromolecules 2022, 23, 2586−2594

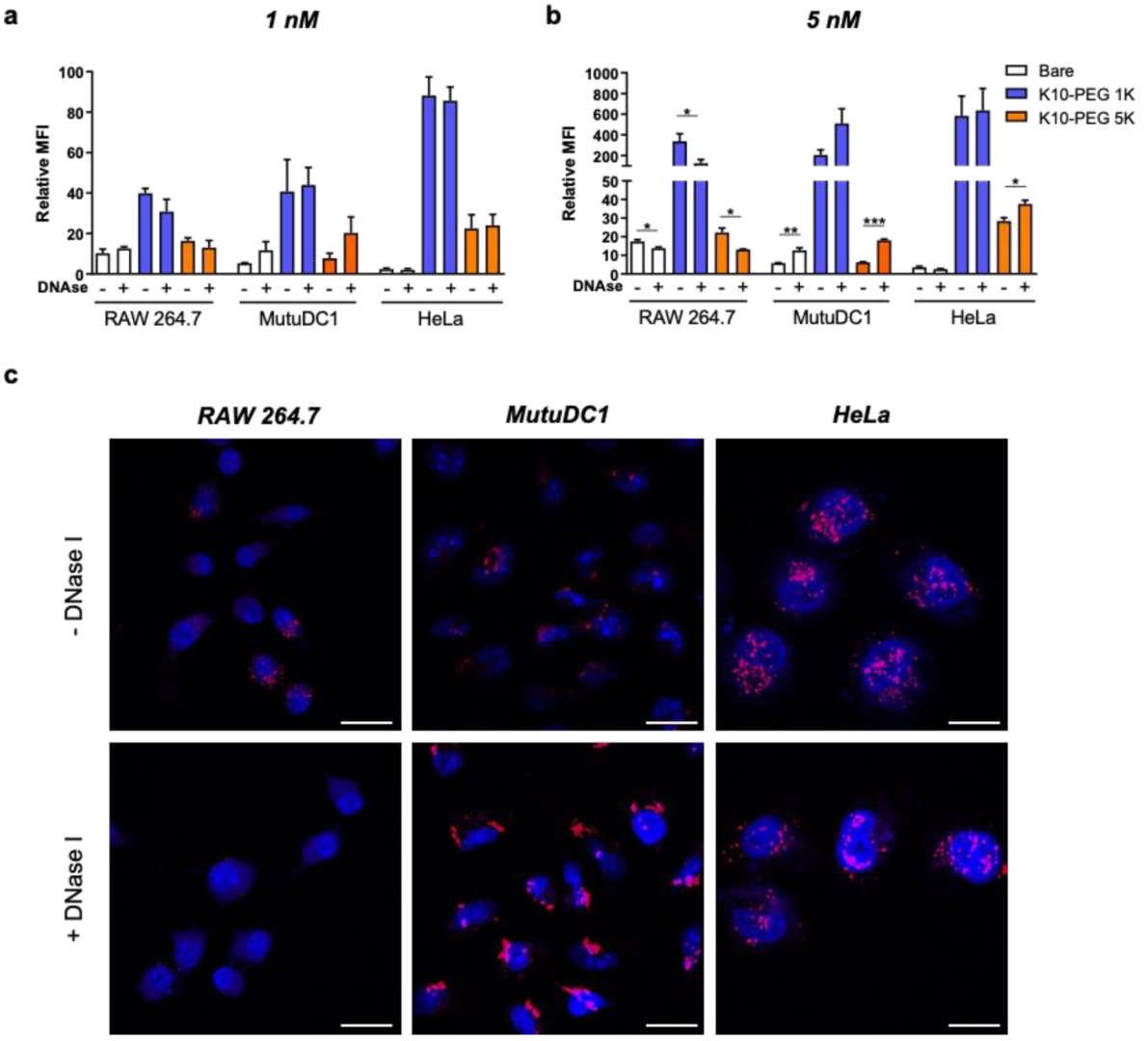

Figure 5. Quantitative analysis of cellular uptake of (a) I-Cy5 disks at 1 nM and (b) 5 nM concentration, coated or not with K10-PEG 1 K and 5 K by RAW 264.7, MutuDC1, and HeLa cell lines, with or without DNase I treatment, assessed by flow cytometry. MFI data are reported compared to the background fluorescence intensity of the corresponding cell line without any treatment as a control. (n = 3). Data are represented as mean +/− SEM values. *P < 0.05; ***P < 0.001, t-test. (c) Confocal microscopy analysis of cellular uptake of I-Cy5 disks at 5 nM concentration, coated with K10-PEG 1 K by RAW264.7, MutuDC1, and HeLa cell lines, with or without DNase I treatment. Overview of confocal images with nuclei in blue (DAPI) and Cy5-labeled disks in red. Full overview of all the samples is reported in Figure S10−S12. Scale bars 20 μm.

and colleagues.[22] We therefore tested the effect of increased concentrations of DNA-Cy5 on the fluorescence within the cells and we observed that for MutuDC1 cells, MFI values were affected in a dose-dependent manner. The same effect was also observed in the other cell lines, but to a lower extent (Figure S9a). Even though the concentrations of DNA-Cy5 tested remained below the uptake threshold established for this study (i.e., the equivalent for 0.25 nM of disks), these results point to the critical importance of keeping DNA-dye strands as control to fluorescence studies, as they could provide false-positive NP uptake data at concentrations higher than 5 nM.

As the cellular uptake rate varies according to the cell type, it is important to differentiate actual uptake to extracellular membrane binding of NPs. This can be realized by treating the cells with a high concentration of DNase I, which clears the extracellular nonspecific binding.[3] However, most *in vitro* studies that focus on DNA origami uptake fail to conclude this step, which we consider essential for the interpretation of the data and prevention of false-positives. To emphasize this issue, we incubated the same three cell lines with bare disks or with disks coated with K10-PEG 1 K or K10-PEG 5 K (N:P ratio 1:1) and after 2 h, a DNase I treatment was performed. Our results show that DNase treatment did not influence the fluorescent signal measured for DNA-dye controls or when NPs were used at 1 nM (Figures S9b and 5a). However, when cells were incubated with NPs at 5 nM, each cell line responded in a different manner to the nuclease treatment: for the RAW 264.7, DNase reduced the Cy5 MFI of the cells, indicating that at this concentration, part of the NPs are sticking to the extracellular membrane. Interestingly, for the MutuDC1 the opposite effect was observed, while for HeLa cells DNase treatment only affected the uptake of K10-PEG 5 K-coated NPs (Figures 5b,c and S10−S12). The surprising shift toward a higher signal in the DCs and cancer cells after treatment with DNase I at high NP concentration suggested that either the partially degrading structures present positively charged structural features to the cells which enhances their uptake, or the DNase I−origami complex interacts in a

https://doi.org/10.1021/acs.biomac.2c00282
Biomacromolecules 2022, 23, 2586−2594

favorable manner with specific uptake receptors in these cell lines. Therefore, particular attention needs to be paid when quantitative studies are performed at high concentrations of DNA origami.

CONCLUSIONS

With DNA as a structural material, the design of NP architectures with an equal size and shape but different surface features can be realized, decoupling variations in the uptake influence of the above-mentioned parameters. Here, we demonstrated that small changes in DNA NP surface parameters (charge, fluorescent dye, and coating) can induce massive cell-dependent uptake differences. While every cell type has its own particularities when interacting with nanomaterials, systematically decoupling the main surface engineering parameters within one platform can significantly help to understand the biointerface when aiming to advance nanotherapeutics.

When designing NPs that will eventually be tested in *in vivo* models, it is critical to ensure that *in vitro* screening studies are carefully designed to avoid future misinterpretation of results or unnecessary use of research animals. Indeed, the great majority of *in vivo* studies focus on the systemic delivery method and NP biodistribution but fail to look at the local target cellular environment.[25,31] Design parameters should be analyzed in detail *in vitro* to understand their effect not only on the cellular target, but on the other cell types that the NP can face during the delivery journey.

Based on our results using DNA-based nanomaterials, we here end with a summary of the most important design considerations when cellular uptake is desired: (1) when delivering to a specific cell type, coating charges need to be analyzed and optimized to obtain cell- and dose-specific uptake; (2) the integration of fluorescent labels instead of H/AH is preferred to prevent their interaction with the cell surface; (3) when using the H/AH strategy to display specific molecules, the effect of the chemical structure on NP uptake by the target cells and neighboring cell types should be verified; (4) for cells with slow uptake kinetics, a stabilizing coating is important to prevent structural degradation and unknown interactions of debris with cells. Equally, coatings are crucial to allow for *in vivo* translation downstream where long-term stability is essential; (5) a concentration of 1 nM or lower *in vitro* to reduce the risk of surface nonspecific binding is recommended. In case a higher concentration is required, the surface-adsorbed portion of the material can be verified with a DNase I treatment.

Each cell type is a complex universe and responds differently to materials presented. In this study, we demonstrated that significant differences occur in the uptake of NPs in three cell types that are commonly used as single examples of DNA origami uptake studies. Surface charge, coating, chemical structure, and concentration were found to all influence the quantitative uptake efficiency of the same original nanomaterial. Therefore, successful cellular uptake of DNA-based nanomaterials is a balance of choosing the right engineering parameters in relation to the cellular population present in the therapeutic target.

ASSOCIATED CONTENT

Supporting Information

The Supporting Information is available free of charge at https://pubs.acs.org/doi/10.1021/acs.biomac.2c00282.

AGC, additional TEM and confocal images, cell viability analysis, additional flow cytometry data, and tables of sequences for the DNA origami disk (PDF)

AUTHOR INFORMATION

Corresponding Author

Maartje M. C. Bastings − *Programmable Biomaterials Laboratory, Institute of Materials/Interfaculty Bioengineering Institute, School of Engineering, Ecole Polytechnique Fédérale Lausanne, Lausanne 1015, Switzerland;* orcid.org/0000-0002-7603-4018; Email: maartje.bastings@epfl.ch

Authors

Marianna M. Koga − *Programmable Biomaterials Laboratory, Institute of Materials/Interfaculty Bioengineering Institute, School of Engineering, Ecole Polytechnique Fédérale Lausanne, Lausanne 1015, Switzerland;* orcid.org/0000-0003-3244-9059

Alice Comberlato − *Programmable Biomaterials Laboratory, Institute of Materials/Interfaculty Bioengineering Institute, School of Engineering, Ecole Polytechnique Fédérale Lausanne, Lausanne 1015, Switzerland*

Hugo J. Rodríguez-Franco − *Programmable Biomaterials Laboratory, Institute of Materials/Interfaculty Bioengineering Institute, School of Engineering, Ecole Polytechnique Fédérale Lausanne, Lausanne 1015, Switzerland*

Complete contact information is available at: https://pubs.acs.org/10.1021/acs.biomac.2c00282

Author Contributions

†M.M.K. and A.C. contributed equally to this work.

Funding

This project has received funding from the European Research Council (ERC) under the European Union's Horizon 2020 research and innovation program (*grant agreement No 948334 InActioN*) and from the "Fondation Pierre Mercier pour la Science."

Notes

The authors declare no competing financial interest.

ACKNOWLEDGMENTS

The authors thank Dr. Jorieke Weiden and Kaltrina Paloja for the insightful discussions and Christine Lavanchy for technical support.

REFERENCES

(1) Seeman, N. C.; Sleiman, H. F. DNA Nanotechnology. *Nat. Rev. Mater.* **2018**, *3*, 17068.

(2) Bila, H.; Kurisinkal, E. E.; Bastings, M. M. C. Engineering a Stable Future for DNA-Origami as a Biomaterial. *Biomater. Sci.* **2019**, *7*, 532−541.

(3) Ponnuswamy, N.; Bastings, M. M. C.; Nathwani, B.; Ryu, J. H.; Chou, L. Y. T.; Vinther, M.; Li, W. A.; Anastassacos, F. M.; Mooney, D. J.; Shih, W. M. Oligolysine-Based Coating Protects DNA Nanostructures from Low-Salt Denaturation and Nuclease Degradation. *Nat. Commun.* **2017**, *8*, 15654.

(4) Yang, Y. R.; Liu, Y.; Yan, H. DNA Nanostructures as Programmable Biomolecular Scaffolds. *Bioconjugate Chem.* **2015**, *26*, 1381−1395.

(5) Li, S.; Jiang, Q.; Liu, S.; Zhang, Y.; Tian, Y.; Song, C.; Wang, J.; Zou, Y.; Anderson, G. J.; Han, J.-Y.; Chang, Y.; Liu, Y.; Zhang, C.; Chen, L.; Zhou, G.; Nie, G.; Yan, H.; Ding, B.; Zhao, Y. A DNA

Nanorobot Functions as a Cancer Therapeutic in Response to a Molecular Trigger in Vivo. *Nat. Biotechnol.* **2018**, *36*, 258−264.
(6) Zhao, S.; Duan, F.; Liu, S.; Wu, T.; Shang, Y.; Tian, R.; Liu, J.; Wang, Z.-G.; Jiang, Q.; Ding, B. Efficient Intracellular Delivery of RNase A Using DNA Origami Carriers. *ACS Appl. Mater. Interfaces* **2019**, *11*, 11112−11118.
(7) Keller, A.; Linko, V. Challenges and Perspectives of DNA Nanostructures in Biomedicine. *Angew. Chem., Int. Ed.* **2020**, *59*, 15818−15833.
(8) Weiden, J.; Bastings, M. M. C. DNA Origami Nanostructures for Controlled Therapeutic Drug Delivery. *Curr. Opin. Colloid Interface Sci.* **2021**, *52*, No. 101411.
(9) Behzadi, S.; Serpooshan, V.; Tao, W.; Hamaly, M. A.; Alkawareek, M. Y.; Dreaden, E. C.; Brown, D.; Alkilany, A. M.; Farokhzad, O. C.; Mahmoudi, M. Cellular Uptake of Nanoparticles: Journey inside the Cell. *Chem. Soc. Rev.* **2017**, *46*, 4218−4244.
(10) Solinas, G.; Germano, G.; Mantovani, A.; Allavena, P. Tumor-Associated Macrophages (TAM) as Major Players of the Cancer-Related Inflammation. *J. Leukocyte Biol.* **2009**, *86*, 1065−1073.
(11) Gustafson, H. H.; Holt-Casper, D.; Grainger, D. W.; Ghandehari, H. Nanoparticle Uptake: The Phagocyte Problem. *Nano Today* **2015**, *10*, 487−510.
(12) Reis e Sousa, C. Dendritic Cells in a Mature Age. *Nat. Rev. Immunol.* **2006**, *6*, 476−483.
(13) Bastings, M. M. C.; Anastassacos, F. M.; Ponnuswamy, N.; Leifer, F. G.; Cuneo, G.; Lin, C.; Ingber, D. E.; Ryu, J. H.; Shih, W. M. Modulation of the Cellular Uptake of DNA Origami through Control over Mass and Shape. *Nano Lett.* **2018**, *18*, 3557−3564.
(14) Wang, P.; Rahman, M. A.; Zhao, Z.; Weiss, K.; Zhang, C.; Chen, Z.; Hurwitz, S. J.; Chen, Z. G.; Shin, D. M.; Ke, Y. Visualization of the Cellular Uptake and Trafficking of DNA Origami Nanostructures in Cancer Cells. *J. Am. Chem. Soc.* **2018**, *140*, 2478−2484.
(15) Hahn, J.; Wickham, S. F. J.; Shih, W. M.; Perrault, S. D. Addressing the Instability of DNA Nanostructures in Tissue Culture. *ACS Nano* **2014**, *8*, 8765−8775.
(16) Wagenbauer, K. F.; Engelhardt, F. A. S.; Stahl, E.; Hechtl, V. K.; Stömmer, P.; Seebacher, F.; Meregalli, L.; Ketterer, P.; Gerling, T.; Dietz, H. How We Make DNA Origami. *ChemBioChem* **2017**, *18*, 1873−1885.
(17) Fuertes Marraco, S. A.; Grosjean, F.; Duval, A.; Rosa, M.; Lavanchy, C.; Ashok, D.; Haller, S.; Otten, L. A.; Steiner, Q.-G.; Descombes, P.; Luber, C. A.; Meissner, F.; Mann, M.; Szeles, L.; Reith, W.; Acha-Orbea, H. Novel Murine Dendritic Cell Lines: A Powerful Auxiliary Tool for Dendritic Cell Research. *Front. Immunol.* **2012**, *3*, 331.
(18) Pigni, M.; Ashok, D.; Stevanin, M.; Acha-Orbea, H. Establishment and Characterization of a Functionally Competent Type 2 Conventional Dendritic Cell Line. *Front. Immunol.* **2018**, *9*, 1912.
(19) Eklund, A. S.; Comberlato, A.; Parish, I. A.; Jungmann, R.; Bastings, M. M. C. Quantification of Strand Accessibility in Biostable DNA Origami with Single-Staple Resolution. *ACS Nano* **2021**, *15*, 17668−17677.
(20) He, C.; Hu, Y.; Yin, L.; Tang, C.; Yin, C. Effects of Particle Size and Surface Charge on Cellular Uptake and Biodistribution of Polymeric Nanoparticles. *Biomaterials* **2010**, *31*, 3657−3666.
(21) Van Vlerken.; et al. Poly(Ethylene Glycol)-Modified Nanocarriers for Tumor-Targeted and Intracellular Delivery. *Pharm. Res.* **2007**, *24*, 1405−1414.
(22) Lacroix, A.; Vengut-Climent, E.; de Rochambeau, D.; Sleiman, H. F. Uptake and Fate of Fluorescently Labeled DNA Nanostructures in Cellular Environments: A Cautionary Tale. *ACS Cent. Sci.* **2019**, *5*, 882−891.
(23) Lühmann, T.; Rimann, M.; Bittermann, A. G.; Hall, H. Cellular Uptake and Intracellular Pathways of PLL-g-PEG-DNA Nanoparticles. *Bioconjugate Chem.* **2008**, *19*, 1907−1916.
(24) Lee, D. S.; Qian, H.; Tay, C. Y.; Leong, D. T. Cellular Processing and Destinies of Artificial DNA Nanostructures. *Chem. Soc. Rev.* **2016**, *45*, 4199−4225.
(25) Hu, Q.; Li, H.; Wang, L.; Gu, H.; Fan, C. DNA Nanotechnology-Enabled Drug Delivery Systems. *Chem. Rev.* **2019**, *119*, 6459−6506.
(26) Donahue, N. D.; et al. Concepts of Nanoparticle Cellular Uptake, Intracellular Trafficking, and Kinetics in Nanomedicine. *Adv. Drug Delivery Rev.* **2019**, *143*, 68−96.
(27) Patel, P. C.; Giljohann, D. A.; Daniel, W. L.; Zheng, D.; Prigodich, A. E.; Mirkin, C. A. Scavenger Receptors Mediate Cellular Uptake of Polyvalent Oligonucleotide-Functionalized Gold Nanoparticles. *Bioconjugate Chem.* **2010**, *21*, 2250−2256.
(28) Gordon, S.; Plüddemann, A. Tissue Macrophages: Heterogeneity and Functions. *BMC Biol.* **2017**, *15*, 53.
(29) Foroozandeh, P.; Aziz, A. A. Insight into Cellular Uptake and Intracellular Trafficking of Nanoparticles. *Nanoscale Res. Lett.* **2018**, *13*, 339.
(30) Kim, H.; Röth, D.; Isoe, Y.; Hayashi, K.; Mochizuki, C.; Kalkum, M.; Nakamura, M. Protein Corona Components of Polyethylene Glycol-Conjugated Organosilica Nanoparticles Modulates Macrophage Uptake. *Colloids Surf., B* **2021**, *199*, No. 111527.
(31) Mitchell, M. J.; Billingsley, M. M.; Haley, R. M.; Wechsler, M. E.; Peppas, N. A.; Langer, R. Engineering Precision Nanoparticles for Drug Delivery. *Nat. Rev. Drug. Discovery* **2021**, *20*, 101−124.

https://doi.org/10.1021/acs.biomac.2c00282
Biomacromolecules 2022, 23, 2586−2594